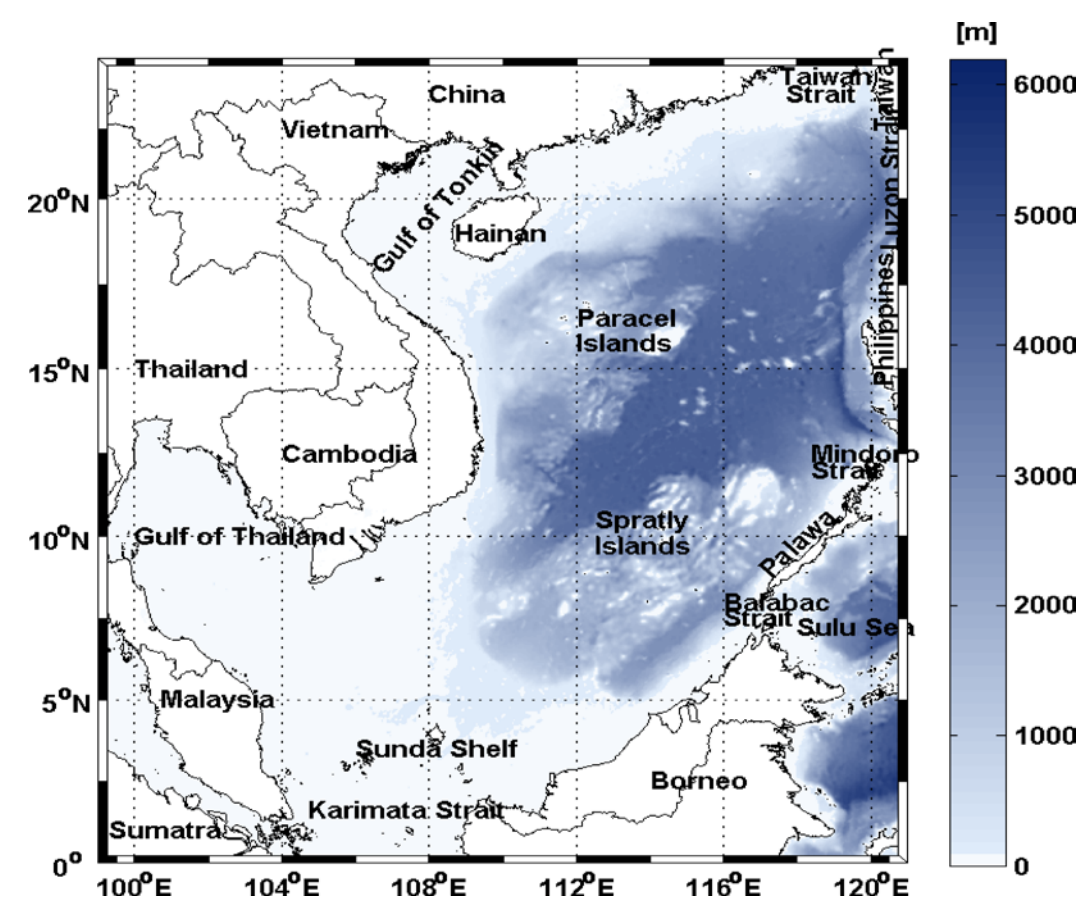


Motivation

The South China Sea (SCS) is located in the tropical region, is affected by monsoon and ENSO, and has complex topography (Fig. 1). Therefore, the temporal and spatial variability of the dynamics in the SCS is very complex.



⇒ To better understand the SCS's dynamics and its relationship with monsoon and ENSO, the analysis of long-term and high-resolution dataset of oceanographic variables should be performed.

Figure 1. Bathymetric map of the South China Sea

Objectives

- Reconstruct a long-term and high-resolution AVHRR Pathfinder SST dataset
- Perform EOF analysis on the reconstructed dataset

Data and Data Processing

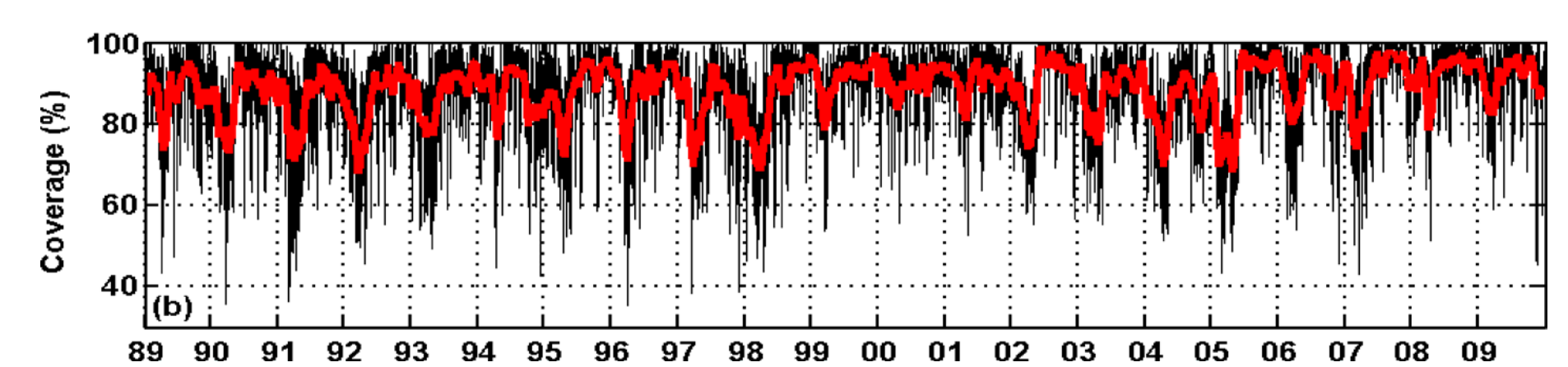
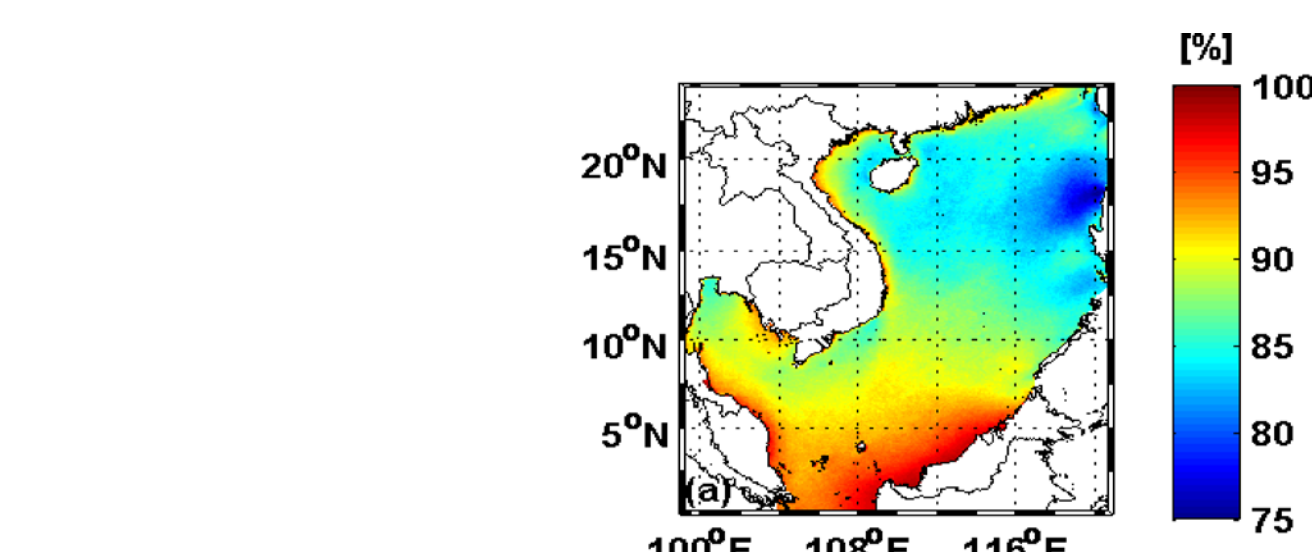


Figure 2. Percentage of cloud-covered AVHRR Pathfinder SST in the SCS: a) Spatial variation of cloud-covered SST, b) Temporal variation of cloud-covered SST (black line) with a thirty-day low-pass filter (red line).

Data: daily night-time 4 km AVHRR Pathfinder SST version 5.0 with high percentage of missing data (Fig. 2)

Data Processing: extract data covering the SCS (7670 images); keep only images containing at least 5% of data; not reconstruct pixels missing more than 95% of the time and consider them as "land"

⇒ **New dataset:** 5119 images (7.19×10^8 pixels, excluding land)

Method

To reconstruct cloud-covered satellite images, we used DINEOF (Data INterpolating Empirical Orthogonal Functions), described in Beckers et al. (2003), Alvera-Azcárate et al. (2005, 2009).

- 1) The initial data input X (5119 images) is obtained by subtracting the temporal and spatial mean and setting the missing data to zero.
- 2) A Singular Value Decomposition of X is performed to calculate the missing data:

$$X_{ij} = \sum_{p=1}^k \rho_p(u_p)_i (v_p^T)_j$$

where i, j are temporal and spatial indices, respectively; k is the retained number of EOF modes; u and v are the spatial and temporal modes, respectively; and ρ are the singular values. This step is repeated until a convergence is reached.

- 3) The optimal number of EOFs will be obtained when the global error between the reconstructed and cross-validation data points is minimum.
- 4) The optimal number of EOFs is used to reconstruct the whole matrix X .

Validation and results

33 modes are retained to reconstruct the SST field.

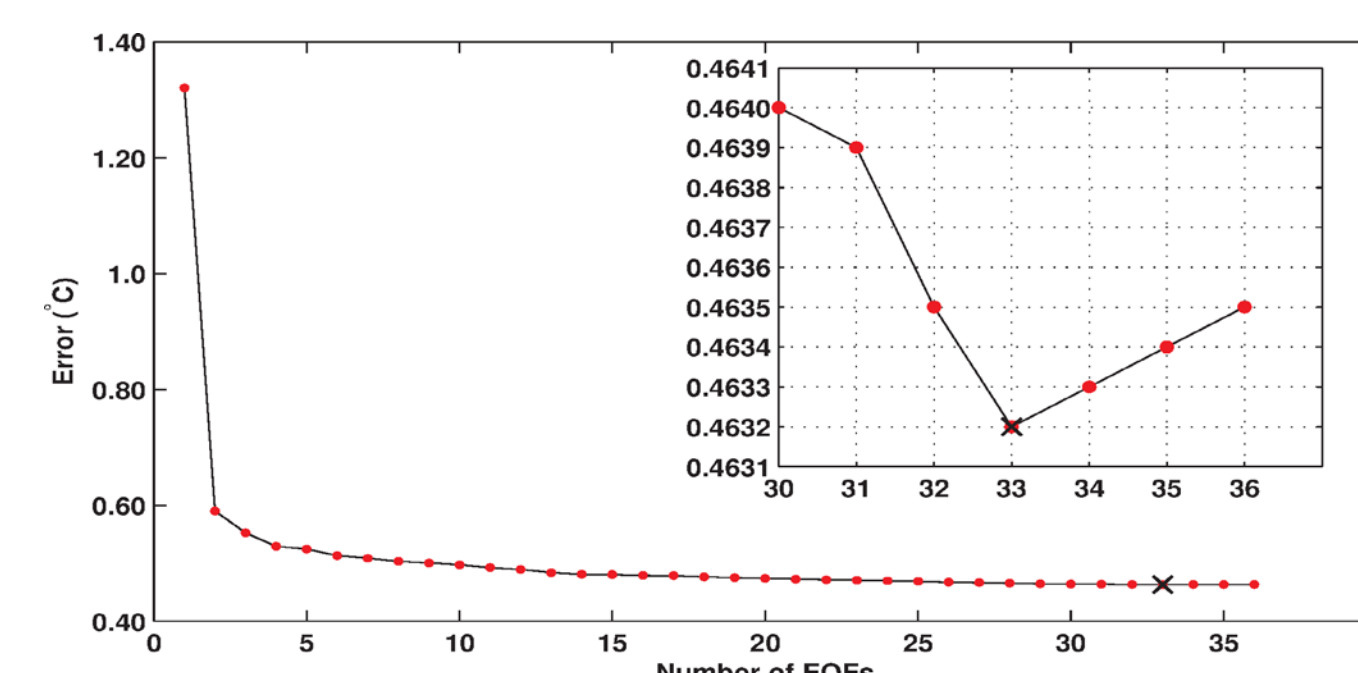


Figure 3. Expected errors obtained from cross-validation. The embedded figure on the upper-right corner zooms in the error with the optimal number of EOFs.

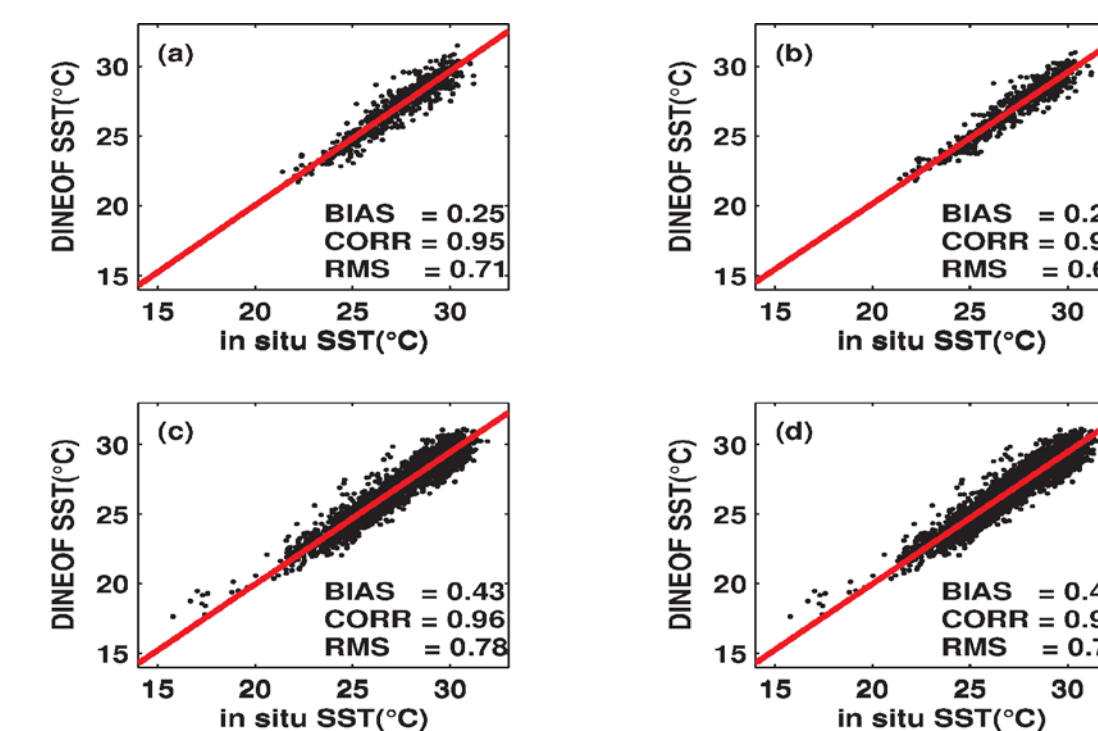


Figure 4. Comparisons between in situ and reconstructed SSTs: a) The original SST with in situ data, b) The reconstructed SST at cloud-free positions with in situ data, c) The reconstructed SST at cloud-covered positions with in situ data, and d) The reconstructed SST at cloud-free and cloud-covered positions with in situ data.

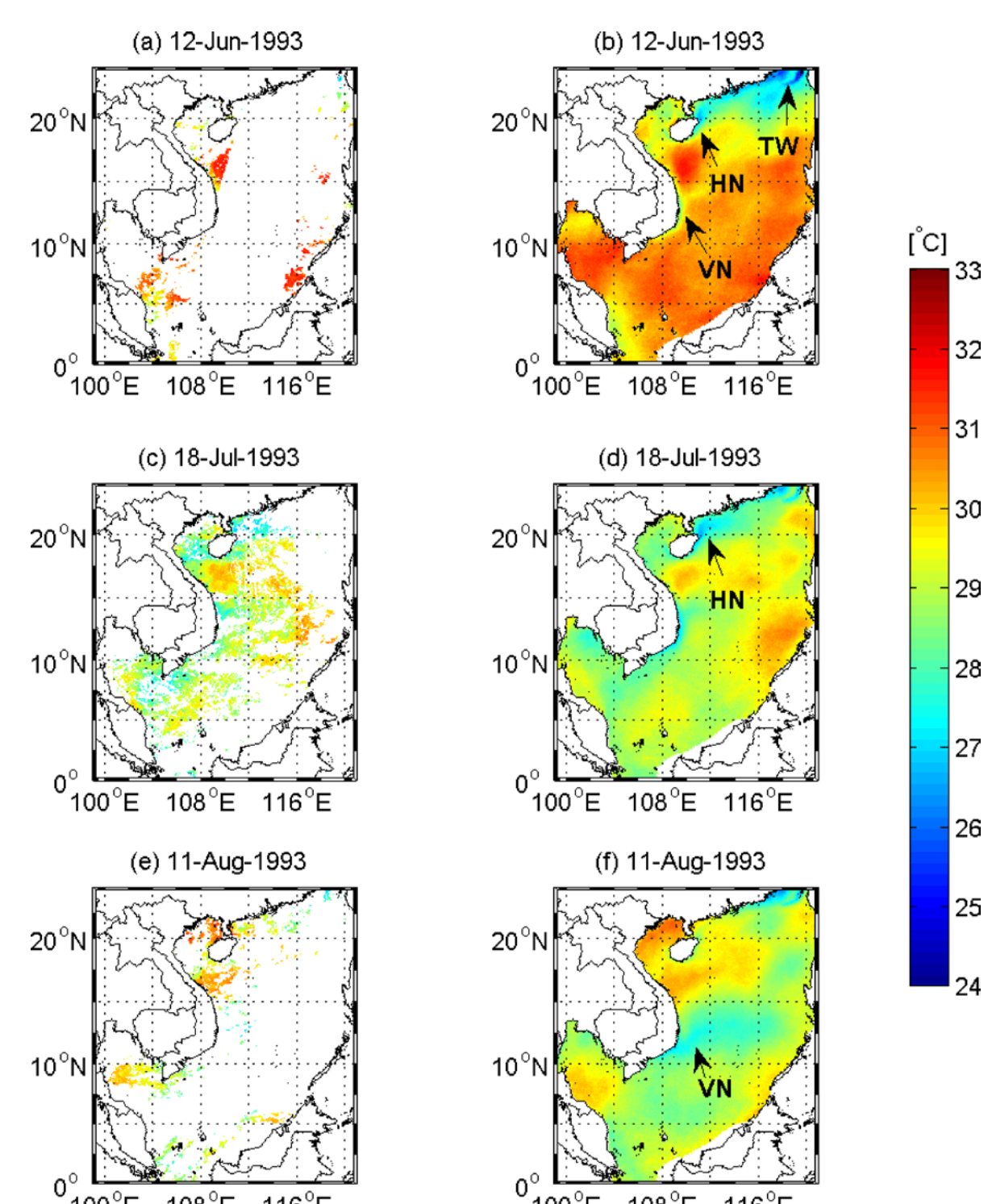


Figure 5. Examples of the reconstructed SST in summer 1993. Figs. (a), (c), and (e) are the original images with high percentage of missing data. Figs. (b), (d), and (f) are the reconstructed images by DINEOF. The arrows and letters in Fig. (b) show three upwelling regions: (1) in the southern Taiwan Strait (TW); (2) around the Hainan Island (HN); and (3) along the southeastern Vietnam (VN). The arrow in Fig. (d) indicates a cold filament in the northeastern Hainan Island. The arrow in Fig. (f) shows a broad and strong cold filament spreading from the VN upwelling.

EOF analysis

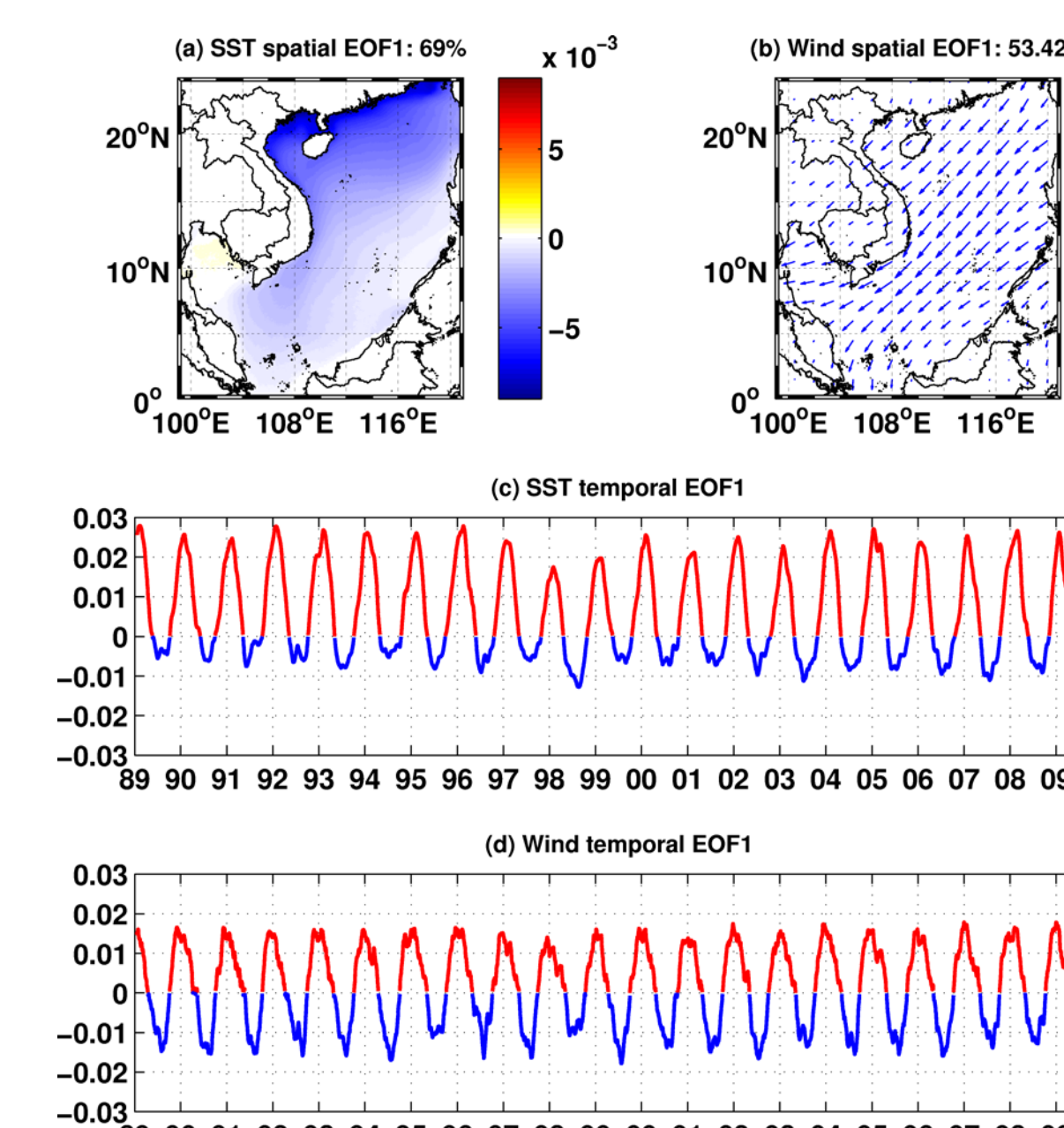


Figure 6. The first SST and surface wind EOFs. Spatial EOF1s: a) SST and b) Surface wind; Temporal EOF1s with a thirty-day low-pass filter: c) SST and d) Surface wind.

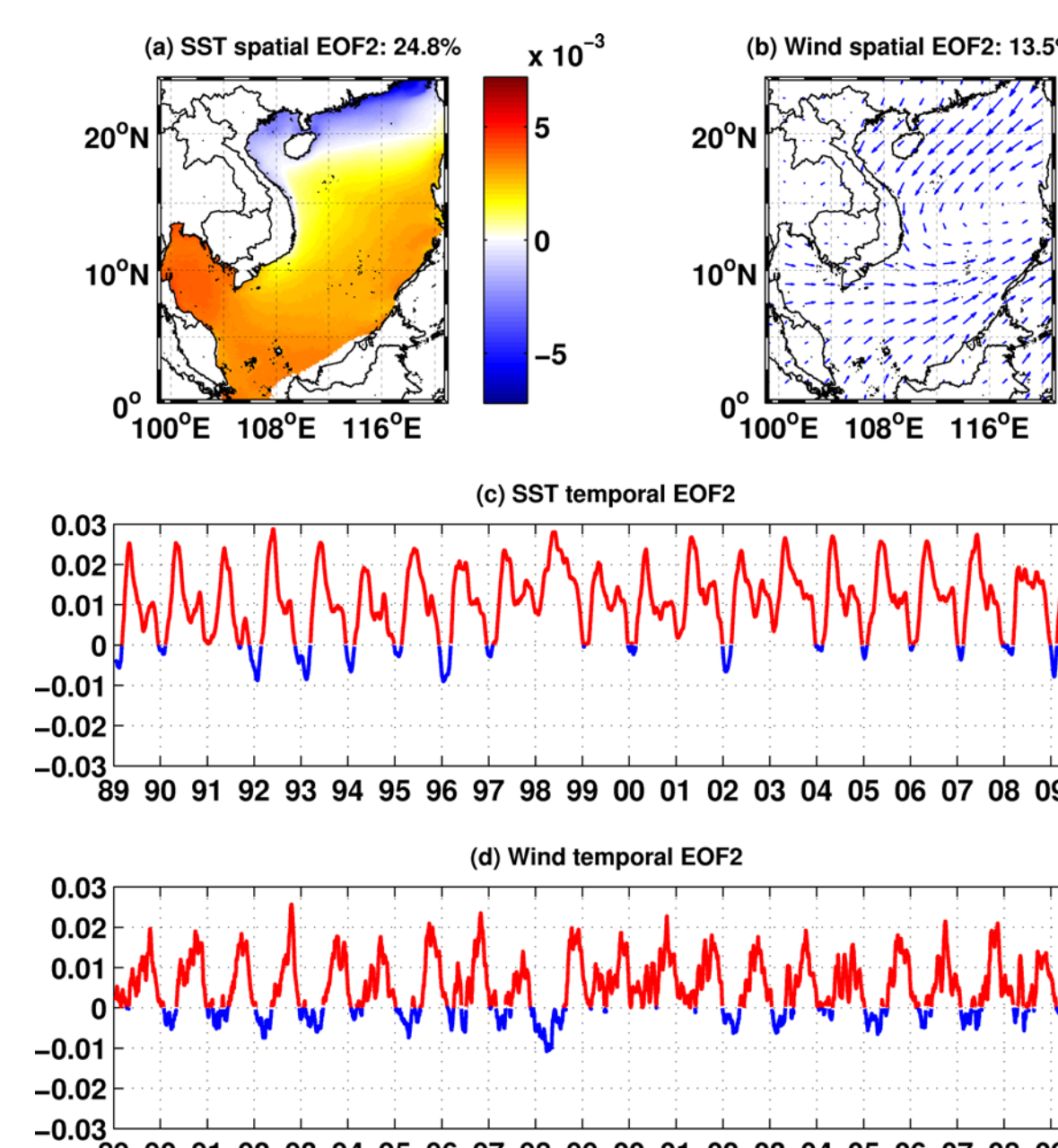


Figure 7. As in Fig. 6 except for the second SST and surface wind EOFs.

The SST EOF1 clearly shows the seasonal variability. It presents a cooling in the whole basin in the northeast monsoon and warming mainly in the northwest of the sea in the southwest monsoon (Figs. 6a, c). The solar insolation, water exchange, topographical features, and monsoon-induced cyclonic circulation are the major factors influencing this pattern. The first SST mode is affected by ENSO (Fig. 8a). The first SST mode shows the signal of the cold tongue in the southeastern coast of Vietnam and the Sunda slope that could not be captured in Chu et al. (1997)'s work.

The SST EOF2 presents the annual variability of the thermal advection along the southwest-northeast diagonal of the basin from two opposite directions (Figs. 7a, c). Under the impact of the anticyclone (Figs. 7b, d), the second SST mode presents an inter-annual variability in response to ENSO (Fig. 9a). The highest values of the SST are located in the Gulf of Thailand and the southwest of the Philippines and the Palawa Island which are different from those in Fang et al. (2006)'s work.

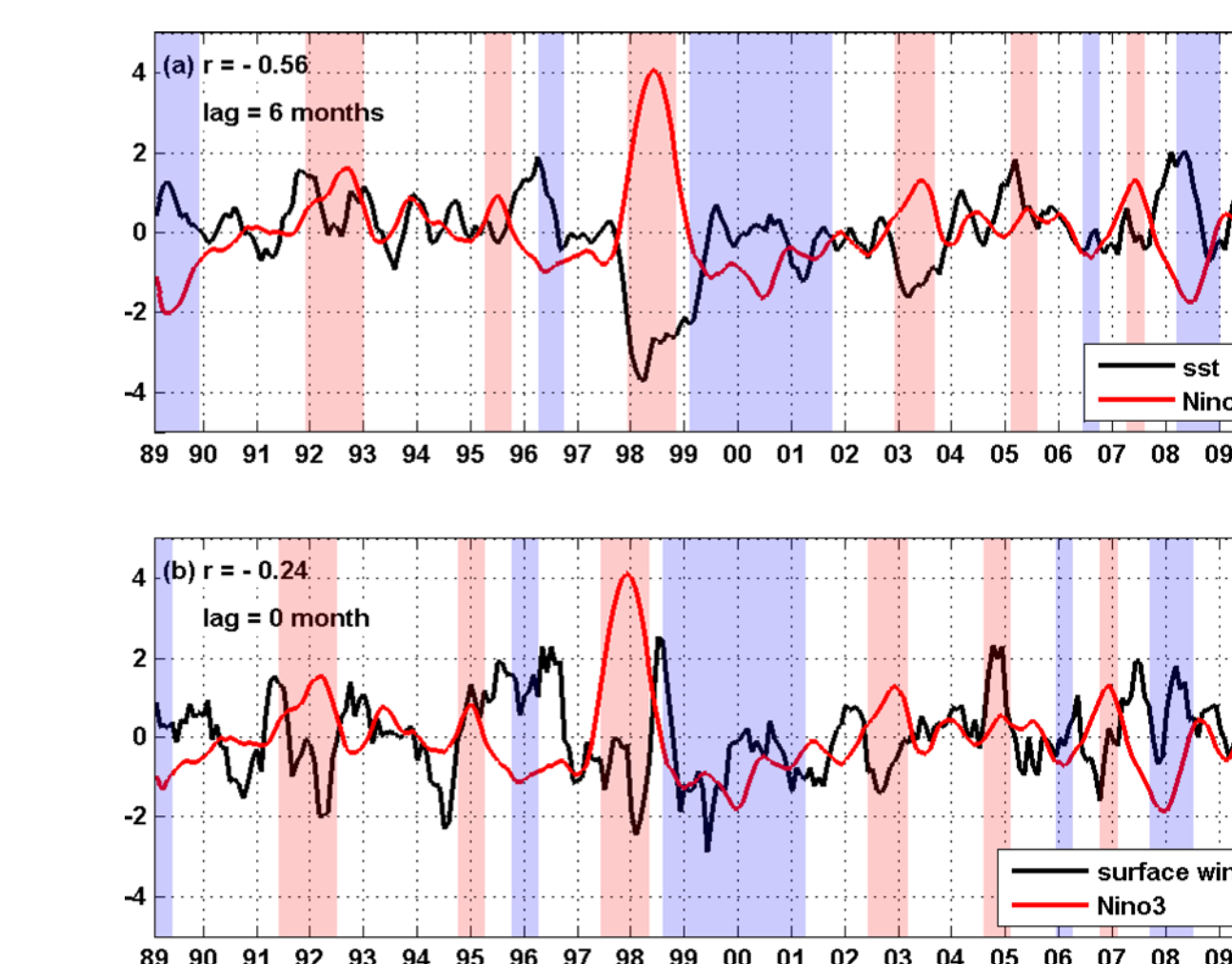


Figure 8. Correlation between the monthly anomalies of the first SST and surface wind temporal EOFs and Nino3 SST. The coloured areas indicating El Niño (pink) and La Niña (blue) are at the lag time corresponding to the maximum correlation coefficient: a) SST and Nino3 with a correlation of -0.56 and a 6-month lag; b) Surface wind and Nino3 with a correlation coefficient of -0.24 and without a lag.

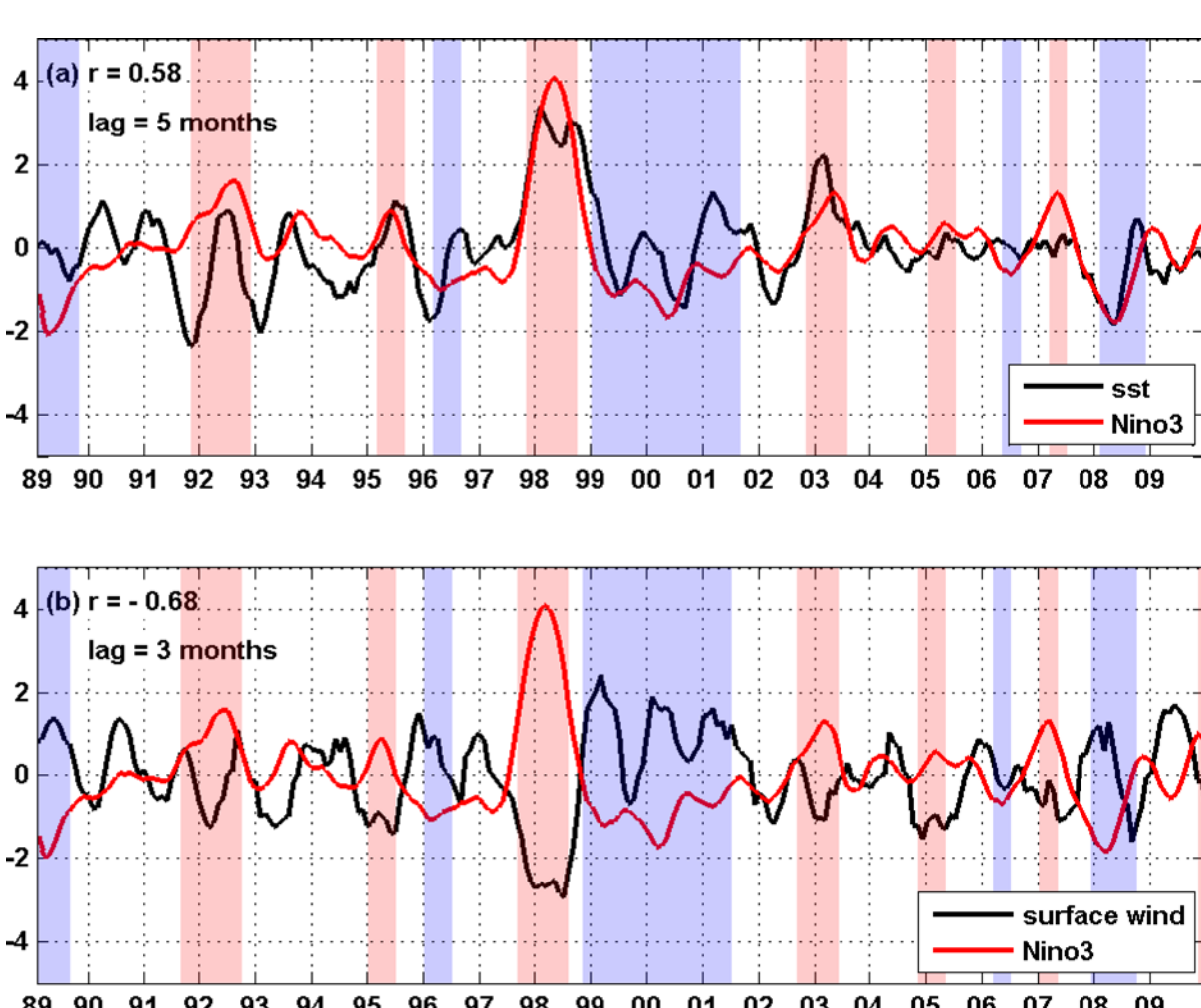


Figure 9. As in Fig. 8 except for the second SST and surface wind EOFs: a) SST and Nino3 with a correlation coefficient of 0.58 and a 5-month lag; b) Surface wind and Nino3 with a correlation coefficient of -0.68 and a 3-month lag.

References

- Alvera-Azcárate, A., A. Barth, M. Rixen, and J.-M. Beckers (2005), Reconstruction of incomplete oceanographic data sets using empirical orthogonal functions: application to the Adriatic sea surface temperature, *Ocean Modelling*, 9 (4), 325-346.
- Alvera-Azcárate, A., A. Barth, D. Sirjacobs, and J.-M. Beckers (2009), Enhancing temporal correlations in EOF expansions for the reconstruction of missing data using DINEOF, *Ocean Science Discussions*, 6 (2), 1547-1568.
- Beckers, J.-M., and M. Rixen (2003), EOF calculations and data filling from incomplete oceanographic datasets, *J. Atmos. Oceanic Technol.*, 20 (10), 1839-1856.
- Chu, P. C., S. Lu., and Y. Chen (1997), Temporal and spatial variabilities of the South China Sea surface temperature anomaly, *Journal of Geophysical Research: Oceans*, 102(C9), 20,937-955.
- Fang, G., H. Chen, Z. Wei, Y. Wang, X. Wang, and C. Li (2006), Trends and interannual variability of the South China Sea surface winds, surface height, and surface temperature in the recent decade, *J. Geophys. Res.*, 111, C11S16.

Acknowledgements

Daily night-time 4 km AVHRR Pathfinder SST data were obtained from the Physical Oceanography Distributed Active Archive Center (PODAAC) at the NASA Jet Propulsion Laboratory. In situ data were downloaded from NOAA National Oceanographic Data Center (NODC), World Ocean Database 2009 (WOD09). Wind data were provided by the European Centre for Medium-Range Weather Forecasts (ECMWF).